Vehicle System Dynamics 4 (1975), pp. 9-41.

The Wheel Shimmy Problem: Its Relationship to Wheel and Road Irregularities

WILLIAM A. PODGORSKI*, ALLAN I. KRAUTER** and RICHARD H. RAND***

ABSTRACT

The equations of motion are derived for a single wheel steerable pneumatic tire system. Included in this system are a built-in wheel wobble and wheel-tire irregularities which produce oscillation of the normal load. Special emphasis is placed on the dynamic characterization of the tire cornering force and aligning torque. The results show that the built-in wheel wobble causes a steady shimmy which is large when the wheel rotation frequency is close to the natural shimmy frequency. The results also show that a normal load oscillation which has a frequency approximately twice the natural shimmy frequency causes a decrease in shimmy stability.

NOMENCLATURE

A	axle
B	top of fork
C_s	suspension damping constant
C_D	rotational viscous damping constant
C	tire constant
C_1	tire constant
C_2	tire constant
C_L	tire constant
CP	contact point
d	axle offset
e	fork center of mass offset
e_1, e_2, e_3	wheel imbalance, out-of-round parameters
E_r, E_i, $E_{max.}$, E	exponential decay rates
F_t	tire cornering force
GC	wheel geometric center

* Research Engineer, Senior, Scientific Research Staff, P.O. Box 2053, Ford Motor Company, Dearborn, Michigan.
** Assistant Professor, Cornell University, Ithaca, New York.
*** Associate Professor, Cornell University, Ithaca, New York.

g	acceleration of gravity
h	height of sprung mass
$(\hat{i}\hat{j}\hat{k})$	unit vectors, inertial system
$(\hat{i}_f\hat{j}_f\hat{k}_f)$	unit vectors, fork system
$(\hat{i}_w\hat{j}_w\hat{k}_w)$	unit vectors, wheel system
$\underset{\approx}{I}_f$	fork inertia tensor
$\underset{\approx}{I}_w$	wheel inertia tensor
$I_{XX_f}, I_{YY_f}, I_{ZZ_f}, I_{XY_f}$	terms in fork inertia tensor
$I_{XX_w}, I_{YY_w}, I_{ZZ_w}$	terms in wheel inertia tensor
K_s	suspension spring rate
K_T	tire spring rate
K_1	tire constant
L_f, L_1, L_2	fork dimensions
L	line of intersection of ground plane and wheel center plane
m_f	fork mass
m_w	wheel mass
M_t	tire aligning torque
N, N_o	normal loads
p	road profile height
P	period of normal load oscillation
R_o	tire radius (unloaded)
R_e	tire rolling radius
r, r_d	deflected tire radii
t	time
T	trail
V_o	initial sprung mass vleocity
$[W]$	fundamental solution matrix
XYZ	inertial co-ordinare system
$X_fY_fZ_f$	fork co-ordinate system
$X_wY_wZ_w$	wheel co-ordinate system
β	wheel out-of-true angle
γ	camber angle
δ	vertical tire deflection
Δ	tire contact patch deflection
η	suspension deflection
ν	caster angle
ψ	fork rotation angle (shimmy angle)

θ	wheel rotation angle
μ_1	tire constant
ψ_t	slip angle
ω_c	wheel rotational frequency
ω_s	shimmy frequency (natural)
ω	frequency of normal load oscillation
λ	road wavelength
δ_p	road profile amplitude
δ_N	magnitude of normal load oscillation
ξ_i	eigenvalues of [W(P)]

1. INTRODUCTION

The problem of wheel shimmy often occurs in vehicles using a steerable pneumatic tire system. This shimmy problem becomes increasingly important as lighter weight steering structures are sought. Although numerous past investigations of the problem have been made, interest in and work on shimmy continues today. Much of this work concerns the characterization of the force and moment response of the pneumatic tire. However, because of the complexity of even the simplest of shimmy problems, applications of such tire characterizations to relatively realistic models of steerable pneumatic tire systems have not been made. In particular, the influence of irregularities in the system on its shimmy behavior have not been treated adequately.

Characterization of tire response has generally been based on one of two theories. One theory follows the work of Von Schlippe and Dietrich [1] in which they modeled the tire as a stretched elastic string. Extensions and modifications to this theory have been made by Smiley [2], Segel [3] and Pacejka [4-6]. Another theory, which uses a somewhat more empirical approach, follows the work of Fromm [7], de Carbon [8], and Moreland [9-10]. In this theory, known as the "Point Contact Theory", the cornering force is related to a linear combination of the slip angle and its time derivative, as well as to a linear combination of the tire deflection and its time derivative. Recent investigations by Collins and Black [11] and Collins [12] have shown that both theories provide accurate predictions of tire response and of wheel shimmy if the parameters used in the tire theories are properly evaluated.

The typical model considered for the steerable pneumatic tire system incorperates a perfect wheel and tire, a smooth road, and a constant speed. At least two authors have considered variations from this simple system. Schrode [13] has found

experimentally that an accelerated wheel system was slightly less stable than a decelerated system. Ho and Lai [14] have analyzed the effect of a static wheel imbalance on wheel shimmy of an aircraft nose wheel. They found a parameteric instability due to coupling between shimmy motion and lateral landing gear strut deflection.

This paper examines the effects on shimmy of several factors not usually included in shimmy analyses. Examined are forced shimmy oscillations caused by an out of true wheel and parametric instabilities associated with normal tire load oscillations. (These normal tire load oscillations can be caused by an imbalanced wheel, an out of round tire, or a rough road.) Also discussed are the effects on shimmy of system accelerations and braking-traction forces.

2. THE MODEL

The model of the aircraft nose landing gear used to determine the effects of the additional factors included in the problem is depicted in Figure 1. Referring to the figure, the pneumatic tire is mounted on the wheel which rotates about the axle.

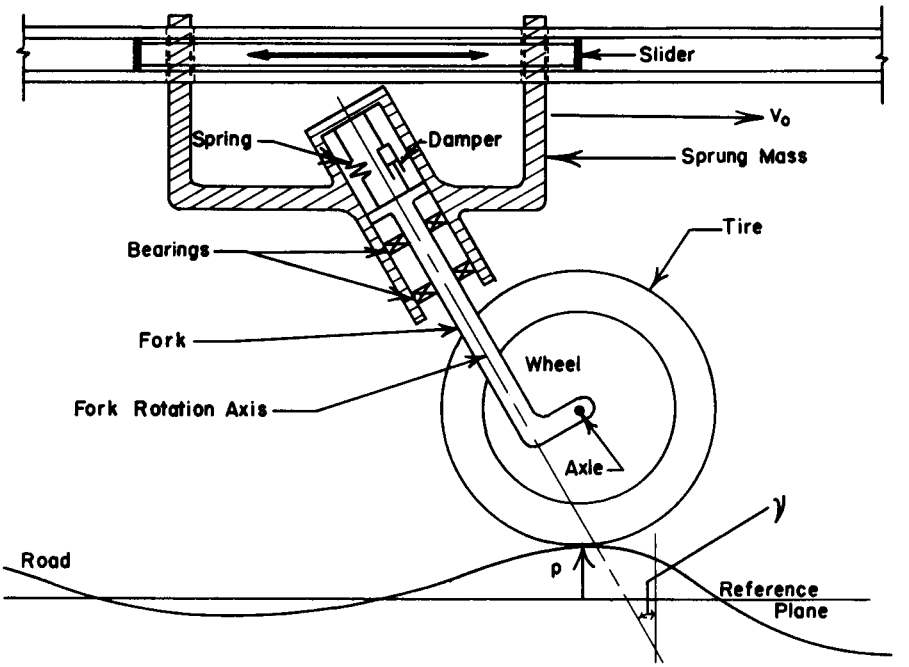

Fig. 1. The Model

The axle is fixed to the fork. The fork rests in bearings which are attached to the sprung mass. The sprung mass translates horizontally at a speed V_o (no pitch). This movement is prescribed. The fork is free to rotate in the bearings and to translate along the rotation axis of the fork. The translation is resisted by a spring and damper. The fork rotation axis makes an angle ν with the vertical.

The road is not considered flat. The height of the ground p (above the reference plane) is a function of position along the road. This road height is assumed to vary as

$$p = \delta p \cos\left[\frac{V_o t}{\lambda}\right] \tag{1}$$

where δp is the magnitude of the road height oscillation and $2\pi\lambda$ is its wavelength.

The system has three degrees of freedom: wheel spin, fork rotation, and fork translation. In addition, the tire contact patch has the freedom to deflect in a direction perpendicular to the plane of the wheel.

Fork and Suspension

The fork and suspension are shown in Figure 2. The suspension spring and damper have linear characteristics; the spring constant is denoted by K_s and the damping constant by C_s. The rotation of the fork is resisted by a viscous damper. This damper also has linear characteristics. The associated damping constant is denoted by C_D. Coulomb friction is neglected throughout the system.

The fork is considered rigid and has mass m_f. The center of mass of the fork lies in the fork plane. This fork plane is that plane defined by the fork rotation axis and the axle attachment point, A. The fork plane is vertical and perpendicular to the reference plane when the fork is pointed directly forward. The axle is perpendicular to the fork plane.

The center of mass of the fork and the axle attachment point are offset from the fork rotation axis by distances e and d, respectively. The total length of the fork is L_f. The distance from the fork center of mass to the top of the fork is L_1, and the distance from the fork center of mass to the bottom of the fork is L_2 ($L_f = L_1+L_2$).

The upper end of the fork is designated as point B. All of the reaction forces and moments of the sprung mass on the fork are assumed to be applied at B. The reaction forces and moments of the wheel on the fork are assumed to be applied at A.

Wheel and Tire

The wheel and tire are shown in Figure 3. The wheel is assumed to have three

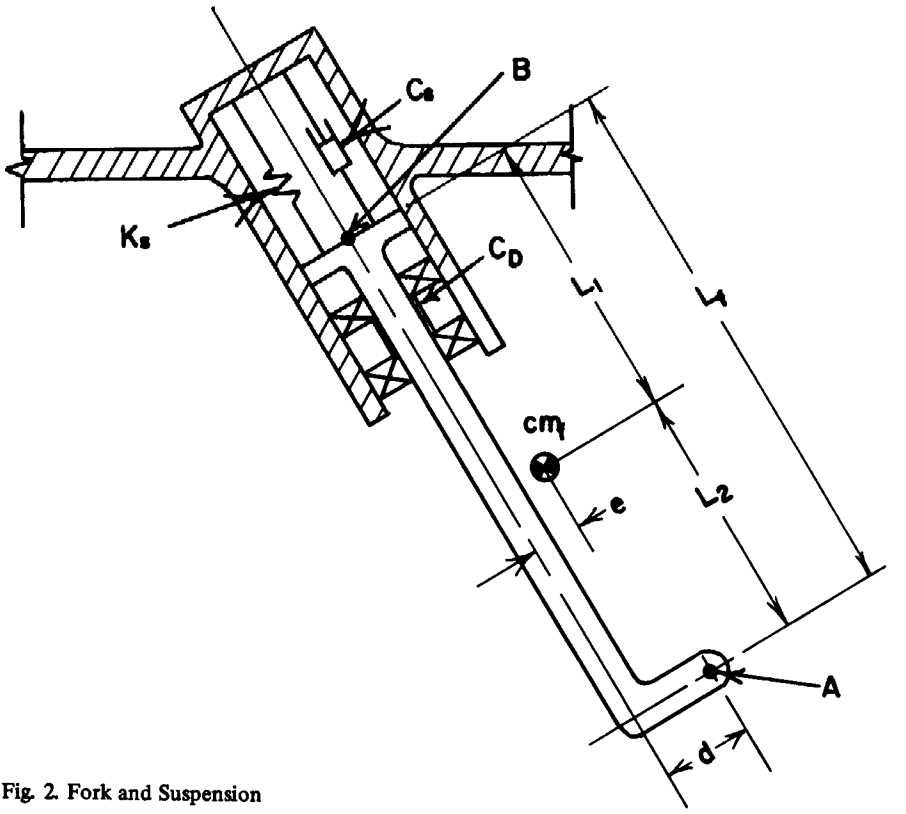

Fig. 2. Fork and Suspension

irregularities whose presence may affect wheel shimmy of the system. The first irregularity involves wheel wobble. The wheel rim is assumed to be perfectly flat. The plane which passes through the center of this rim will be referred to as the wheel center plane. On a perfect wheel the wheel center plane would coincide with the fork plane and would be perpendicular to the axis of rotation of the wheel. In the wheel under consideration, however, the wheel center plane is tilted with respect to the fork plane by an angle β, which is small (see Figure 3). This gives the wheel a small built-in wobble which is often present in spoked wheels.

The second and third irregularities involve wheel balance and roundness. The center of mass of the wheel is offset from A, the center of rotation, by a distance $\sqrt{e_1^2 + e_2^2}$, thus making the wheel unbalanced. The geometric center of the wheel and tire is also offset from A, by a distance e_3, making the tire "out of round."

The wheel and tire are perfectly circular (with center at GC) and are symmetric about the wheel center plane. The tire is assumed to be vertically flexible, the

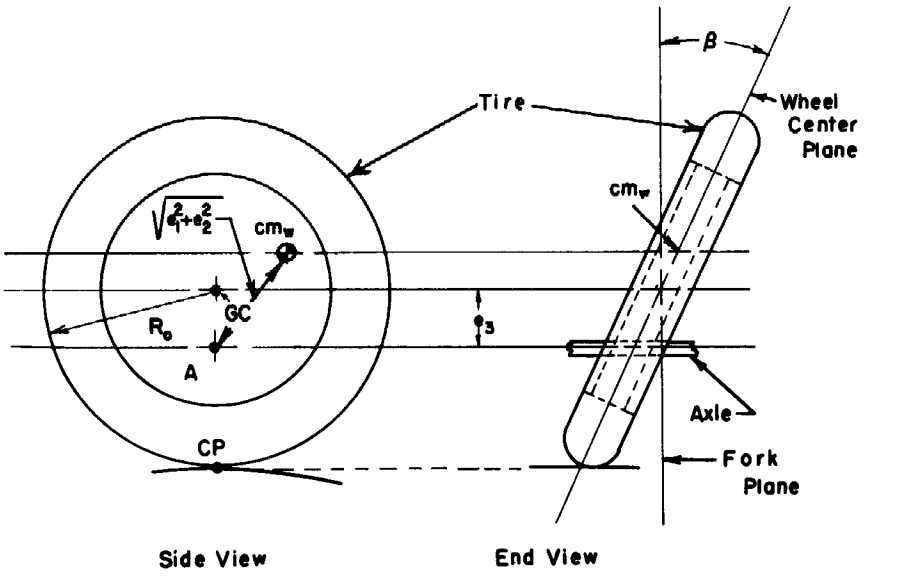

Fig. 3. Wheel and Tire

stiffness being measured by the tire spring constant for vertical deflection, K_T. Contact between the road and the tire is assumed to be made at the point CP, the tire contact point.

The dimensions which describe the tire are the unloaded radius R_o and the effective radius R_e. The reactions on the tire from the road are the cornering force, normal force, and aligning torque. The mass of the wheel is m_w.

Co-ordinate Systems

Three co-ordinate systems are used to obtain the equations of motion for the model. The XYZ system (Fig. 4) is inertial and is fixed to the ground. The X axis of the system is horizontal and lies in the reference plane. The Y axis points vertically upward from the ground. The Z axis lies in the reference plane and is defined such that X, Y, and Z form a right-handed system. The orientation is chosen such that the tire force sign convention of [11] is followed.

The $X_fY_fZ_f$ system, or fork coordinate system, is fixed to the fork with the origin at the fork center of mass. The X_f axis lies in the fork plane and is perpendicular to the fork axis of rotation. The Y_f axis lies in the fork plane, is parallel to the fork axis of rotation, and points up. The Z_f axis is perpendicular to the fork plane and is defined such that X_f, Y_f, and Z_f form a right-handed system.

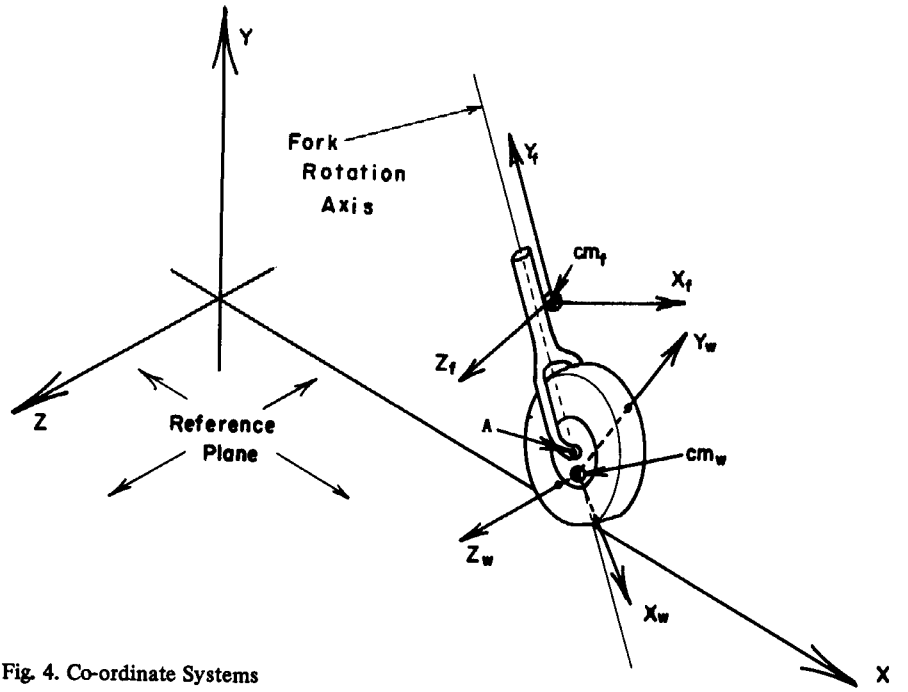

Fig. 4. Co-ordinate Systems

The $X_wY_wZ_w$ system, or wheel coordinate system, is fixed to the wheel with the origin at the wheel center of mass. The X_w and Y_w axes lie in the wheel center plane and are principal axes of the wheel. The Z_w axis is perpendicular to the wheel center plane and is defined such that the X_w, Y_w, and Z_w axes form a right-handed system. For a wheel with no irregularities the Z_w axis is parallel to the Z_f axis.

Transformations relating the three coordinate systems can be obtained by making successive rotations about coordinate axes. The transformation between XYZ and $X_fY_fZ_f$ is obtained by two rotations. The first rotation is about the Z axis by angle ν, the caster angle. The second rotation is about the fork rotation axis by angle ψ, the shimmy angle. This angle is one of the generalized coordinates of the system.

The transformation between $X_fY_fZ_f$ and $X_wY_wZ_w$ is also obtained by two rotations. The first rotation is about the Z_f axis by angle θ. (which measures wheel spin and is a generalized co-ordinate of the system) The second rotation is about one of the principal axes of the wheel by angle β. The angle β measures the magnitude of the wheel wobble irregularity.

Sets of unit vectors $(\hat{i},\hat{j},\hat{k})$, $(\hat{i}_f,\hat{j}_f,\hat{k}_f)$, and $(\hat{i}_w,\hat{j}_w,\hat{k}_w)$ are defined for the coordinate systems XYZ, $X_fY_fZ_f$, and $X_wY_wZ_w$, respectively. Relationships between sets of unit vectors can be obtained from the successive rotations described above.

Fork and Wheel Intertia

The inertia tensor for the fork is defined with respect to the fork co-ordinate system. This inertia tensor, I_f, is

$$\underset{\approx}{I}_f = \begin{bmatrix} I_{XX_f} & I_{XY_f} & 0 \\ I_{XY_f} & I_{YY_f} & 0 \\ 0 & 0 & I_{ZZ_f} \end{bmatrix} \tag{2}$$

The inertia tensor for the wheel is defined with respect to the wheel coordinate system. This wheel tensor is

$$\underset{\approx}{I}_w = \begin{bmatrix} I_{XX_w} & 0 & 0 \\ 0 & I_{YY_w} & 0 \\ 0 & 0 & I_{ZZ_w} \end{bmatrix} \tag{3}$$

Tire Force and Moment Characterization

The reactions from the road on the tire are shown in Figure 5. These reactions are the normal load, N, the cornering force, F_t, and the aligning torque, M_t. The tire's overturning moment, rolling resistance moment, and braking-traction force are not considered. All of these reactions are assumed to be exerted at the tire-road contact point, CP, which is assumed to be at the center of the tire's contact patch. The tire contact point is allowed to deflect with respect to the wheel. This deflection is defined by Δ, measured perpendicularly to line L. The line L is the intersection of the ground plane and the wheel centerplane. The cornering force acts in the ground plane, perpendicular to L. The normal load and aligning torque act vertically.

The normal load is assumed to be a linear function of the tire deflection, δ. This assumed function is

$$N = K_T\delta \tag{4}$$

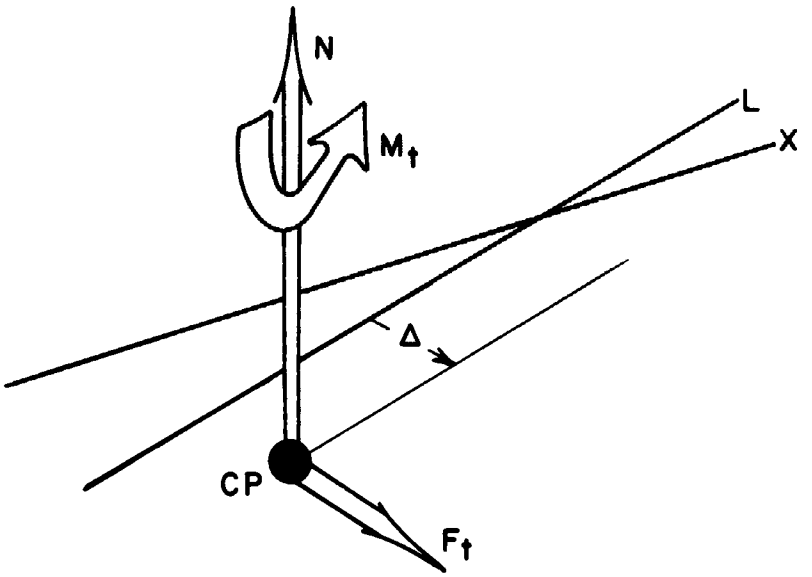

Fig. 5. Tire Forces and Moment

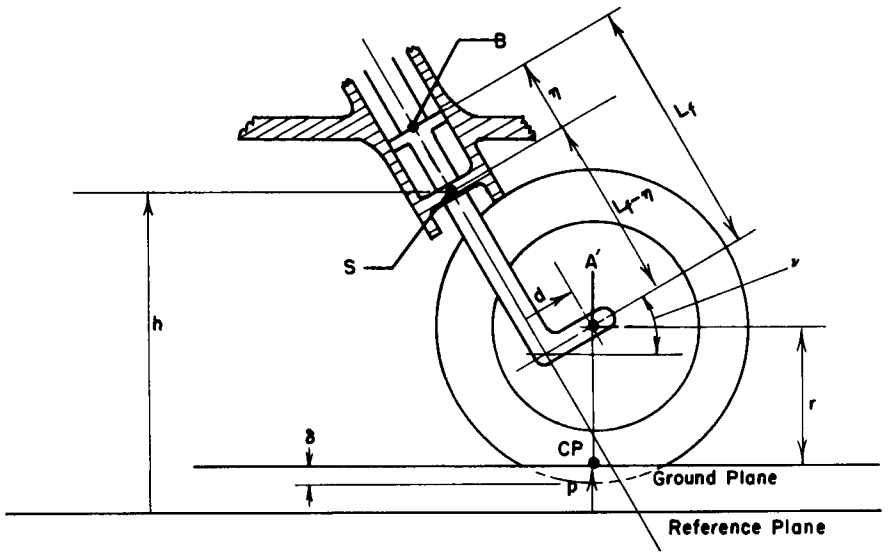

Fig. 6. Tire Deflection

The tire deflection, δ, is shown in Figure 6. This deflection is the difference between the axle to ground plane distance, r, and the distance between the axle and the bottom of the unloaded tire. Taking into account the out-of-roundness of the tire, the deflection δ is

$$\delta = R_o + e_3 \sin\theta - r \tag{5}$$

Distance r is obtained from Figure 6 and is

$$r = (h-p) - (L_f - \eta)\cos\nu + d\sin\nu \tag{6}$$

where h is the height of point S on the sprung mass above the reference plane.

The method used to characterize the tire cornering force and aligning torque is critical in any analysis of wheel shimmy. In this work the contact point theory of Moreland [9,10] and Collins [11] is adopted. According to this theory, relationships which describe the cornering force, F_t, and the aligning torque, M_t, are

$$F_t = \frac{1}{C}[\psi_t + C_1\dot{\psi}_t - C_2\gamma] \tag{7}$$

and

$$M_t = \mu_1\psi_t \tag{8}$$

where ψ_t is the slip angle and γ is the camber angle. The camber angle is the angle between the wheel center plane and the vertical

$$\gamma = \psi\sin\nu + \beta(\sin\nu\sin\theta - \cos\nu\cos\theta) \tag{9}$$

The tire slip angle is shown in Figure 7. The slip angle is defined as the angle between the tire contact point velocity, V_{CP}, and the direction in which the tire is pointing, L. The slip angle is given by

$$\psi_t = -\psi\cos\nu - \beta(\cos\nu\sin\theta + \sin\nu\cos\theta) - \frac{\dot{\Delta} + r\dot{\gamma} + d\dot{\psi}}{V_o} \tag{10}$$

When the above relationships for the camber and slip angles are substituted into Equation (7) and (8), new relationships for the cornering force and aligning torque result. These new relationships, however, contain the tire deflection variable Δ, and its derivatives. From experimental evidence, Moreland [9, 10] and Collins [11] have proposed that the cornering force is also related to the tire deflection by

$$F_t = K_L\Delta + C_L\dot{\Delta} \tag{11}$$

The above expression (11) plus the expressions which result from the combination of (7), (8), (9) and (10) complete the characterization of the tire cornering force and aligning torque.

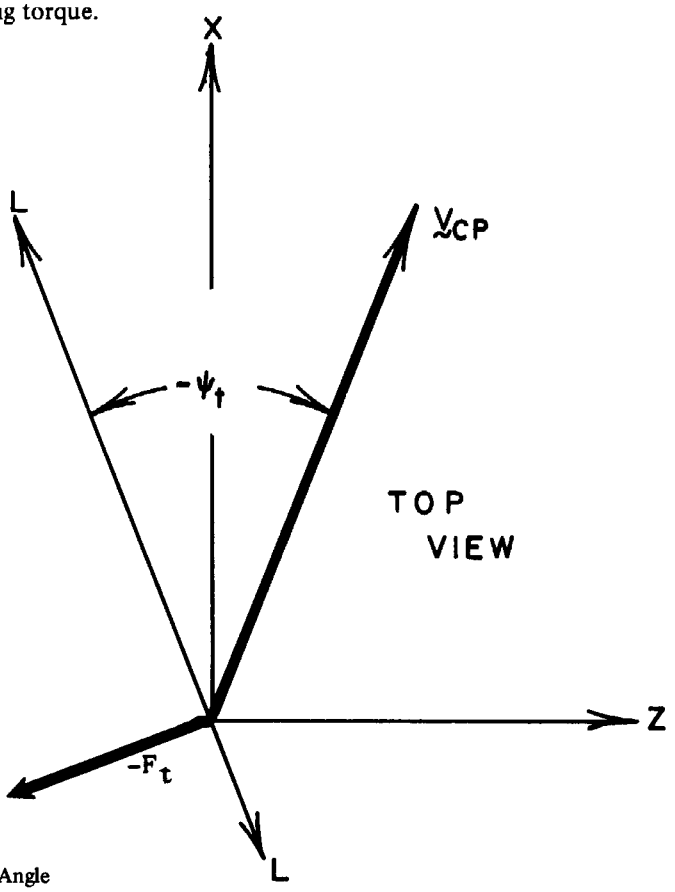

Fig. 7. Slip Angle

Equations of Motion (State Variable Formulation)

Translational and rotational equations of motion for the model are derived in [15]. The equations contain unknown constraint forces and torques. These constraint reactions act between the fork and the sprung mass and between the fork and the wheel. Elimination of the constraint reactions from the equations of motion results in three coupled, second order differential equations involving the three generalized coordinates ψ, η, and θ, as well as N, F_t, and M_t. These equations are given below and are written in a linearized form. The linearization is obtained by assuming that ψ, $\dot{\psi}$, and β are small.

The first of the set of three coupled equations in the generalized coordinates is basically an equation for fork rotation, ψ. This equation is

$$[I_\psi]\frac{d\dot{\psi}}{dt} + [\beta\cos\theta\,(I_{YY_w} - I_{ZZ_w})]\frac{d\dot{\theta}}{dt} = M_t\cos\nu + A_3 N\sin\nu +$$

$$(B_1 - A_1 - d)F_Z - C_D\dot{\psi} + (dm_w + e\,m_f - B_1 m_w)\,g\psi\sin\nu + \beta\dot{\theta}^2(I_{YY_w} - I_{ZZ_w})\sin\theta +$$

$$\dot{\psi}\dot{\theta}(B_2 m_w[B_1 - d] - \sin\theta\cos\theta\,[I_{XX_w} - I_{YY_w}]) \qquad (12)$$

where

$$I_\psi = I_{XX_w}\sin^2\theta + I_{YY_w}\cos^2\theta + I_{YY_f} + d^2 m_w + e^2 m_f - B_1 m_w d$$

$$B_1 = e_1\cos\theta - e_2\sin\theta$$

$$B_2 = e_1\sin\theta + e_2\cos\theta$$

$$A_1 = -r\sin\nu - e_3\cos\nu\cos\theta + B_1$$

$$A_3 = -r\psi\sin\nu + r\gamma + \Delta$$

$$F_Z = F_t + N\psi\sin\nu$$

The second of the three equations is an equation for the suspension deflection, η, and is

$$[m_f + m_w]\frac{d\dot{\eta}}{dt} - [B_1 m_w d]\frac{d\dot{\theta}}{dt} = -(m_f + m_w)\,g\sin\nu - B_2 m_w\dot{\theta}^2 -$$

$$- C_s\dot{\eta} - K_s\eta + N\cos\nu \qquad (13)$$

The last of the three equations is basically an equation for wheel rotation. It is

$$[B_1 m_f]\frac{d\dot{\eta}}{dt} + [I_\theta]\frac{d\dot{\theta}}{dt} + [\beta\cos\theta\,(I_{YY_w} - I_{ZZ_w})]\frac{d\dot{\psi}}{dt}$$

$$= (B_2 - A_2)N\sin\nu + A_1 N\cos\nu - B_1(C_s\dot{\eta} + K_s\eta) - B_2 m_w(g\sin\nu + B_1\dot{\theta}^2) \qquad (14)$$

$$+ B_1 m_f g\cos\nu + \psi(B_2 m_w d + \sin\theta\cos\theta\,[I_{XX_w} - I_{YY_w}]) + M_t\Psi\sin\upsilon$$

where

$$I_\theta = I_{ZZ_w} + m_w B_2^2$$

and

$$A_2 = -r\cos\nu + e_3\sin\nu\cos\theta + B_2$$

Equations (12), (13), (14), and the equations which result from the combination of equations (7)-(11) describe the motion of the system. This set of equations is of eighth order. The state of the system at any time is specified by eight quantities – the eight state variables Δ, ψ_t, ψ, η, θ, $\dot{\psi}$, $\dot{\eta}$, and $\dot{\theta}$. The state variable formulation of the equations of motion is developed below.

In the state variable formulation of the problem expressions are required for the time derivative of each state variable in terms of the other state variables. Equations (12), (13), and (14) and the differential relations

$$\frac{d\psi}{dt} = \dot{\psi} \tag{15}$$

$$\frac{d\eta}{dt} = \dot{\eta} \tag{16}$$

$$\frac{d\theta}{dt} = \dot{\theta} \tag{17}$$

provide six of the eight expressions. Expressions for $d\Delta/dt$ and $d\psi_t/dt$ are required to complete the state variable formulation of the problem. An expression for $d\Delta/dt$ is obtained from Equation 10. After rearranging, this expression is

$$\frac{d\Delta}{dt} = -V_o[\psi_t + \tau] - \dot{\gamma}r] \tag{18}$$

where

$$\tau = \psi\cos\nu + \beta[\cos\nu\sin\theta + \sin\nu\cos\theta]$$

The expression for $d\psi_t/dt$ is obtained by first substituting $\dot{\Delta}$ from Equation 18 into Equation 11 to give

$$F_t = K_1\Delta - C_L[V_o(\psi_t + \tau) + \dot{\gamma}r] \tag{19}$$

then by equating F_t from Equation 7 to F_t from Equation 19. Rearrangement of the resulting expression gives

$$\frac{d\psi_t}{dt} = \frac{1}{C_1}[CK_1\Delta - \psi_t - C_2\gamma - CC_2[V_o(\psi_t + \tau) + \dot{\gamma}r]] \tag{20}$$

Equations (12) – (17), (18), and (20) comprise the state variable formulation of the problem. This set of equations can be written as

$$[U]\frac{d\underset{\sim}{X}}{dt} = \underset{\sim}{f}(\underset{\sim}{X}, t) \tag{21}$$

where X is the [8x1] state vector whose components are Δ, ψ_t, ψ, η, θ, $\dot{\psi}$, $\dot{\eta}$, $\dot{\theta}$, and f(X,t) is the [8x1] vector whose components are the eight righthand sides of Equations (18), (20), (15), (16), (17), (12), (13) and (14). In Equation (21), the [8x8] matrix* [U] is given by

$$[U] = \begin{bmatrix} 1 & 0 & 0 & 0 & 0 & 0 & 0 & 0 \\ 0 & 1 & 0 & 0 & 0 & 0 & 0 & 0 \\ 0 & 0 & 1 & 0 & 0 & 0 & 0 & 0 \\ 0 & 0 & 0 & 1 & 0 & 0 & 0 & 0 \\ 0 & 0 & 0 & 0 & 1 & 0 & 0 & 0 \\ 0 & 0 & 0 & 0 & 0 & \multicolumn{3}{c}{\multirow{3}{*}{U_1}} \\ 0 & 0 & 0 & 0 & 0 & & & \\ 0 & 0 & 0 & 0 & 0 & & & \end{bmatrix}$$

where $[U_1]$ is the [3x3] matrix

$$[U_1] = \begin{bmatrix} I_\psi & 0 & \beta\cos\theta\,(I_{YY_w} - I_{ZZ_w}) \\ 0 & (m_f + m_w) & -B_1 m_w \\ \beta\cos\theta\,(I_{YY_w} - I_{ZZ_w}) & B_1 m_f & I_\theta \end{bmatrix}$$

3. RESULTS

The results presented in this section were obtained by numerical integration of Equation (21) and by application of linear stability** techniques to simplified forms of that equation. The values of the parameters were chosen to represent the front wheel and suspension of a tricycle aircraft landing gear. These values are given in Table 1.

---

* The determinant of [U] is $(m_f+m_w)\, I_\psi I_\theta + B_1^2 m_f m_w I_\psi$. This determinant is nonzero for physically reasonable systems.

** The shimmy will be said to be stable if it remains bounded as $t \to \infty$.

Table 1.

Parameters For Aircraft Nose Landing Gear

I. *Masses and Inertias*

m_f	:	0.07	(lb.sec.^{2}/in.)
m_w	:	0.145	(lb.sec.^{2}/in.)
I_{YY_f}	:	0.4	(lb.sec.^{2}in.)
I_{XY_f}	:	0.0	(lb.sec.^{2}in.)
I_{XX_w}	:	6.5	(lb.sec.^{2}in.)
I_{YY_w}	:	6.5	(lb.sec.^{2}in.)
I_{ZZ_w}	:	11.0	(lb.sec.^{2}in.)

II. *Dimensions*

L_1	:	15.0	(in.)
L_2	:	15.0	(in.)
e	:	0.0	(in.)
R_o	:	13.5	(in.)

III. *Spring and Damper Characteristics*

K_s	:	750.0	(lb./in.)
C_s	:	45.0	(lb.sec./in.)
C_D	:	0.0	(in.lb.sec.)

IV. *Caster Angle*

ν	:	$27^\bullet$

Seven tire parameters are necessary to determine the three tire reactions: normal load, cornering force, and aligning torque. The tire spring rate K_T is used in the determination of the normal load. For the physical system chosen, an 18"x5 1/2" aircraft tire was used. The value of K_T has been obtained for this tire by Smiley

[16] and is listed in Table 2. The remaining six parameters, C, C_1, C_2, μ_1, K_1, and C_L are used in the contact point tire theory to determine the cornering force and aligning torque. These parameters are assumed to be functions of the normal load, N, and of the speed, V_o. The assumed functions are

$$\begin{aligned} C &= C_f + C_v(N-3100) \\ C_1 &= C_{1f} + C_{1v}(N-3100) + [C_{1fv} + C_{1vv}(N-3100)]V_o \\ C_2 &= C_{2f} + C_{2v}(N-3100) \\ \mu_1 &= \mu_{1f} + \mu_{1v}(N-3100) \\ K_1 &= K_{1f} + K_{1v}(N-3100) \\ C_L &= C_{Lf} + C_{Lv}(N-3100) \end{aligned} \tag{22}$$

Table 2.

Tire Constants

K_T	:	1350.0 (lbs./in.)
C_f	:	$.75 \times 10^{-4}$ (rad./lb.)
C_v	:	$.33548 \times 10^{-7}$ (rad.)
C_{1f}	:	0.0 (sec./rad.)
C_{1v}	:	$-.86021 \times 10^{-7}$ (sec./rad.lb.)
C_{1fv}	:	$.11 \times 10^{-5}$ (sec.^{2}/in.)
C_{1vv}	:	$.12473 \times 10^{-8}$ (sec.^{2}/in.lb.)
C_{2f}	:	.1 (rad.)
C_{2v}	:	0. (1/lb.)
μ_{1f}	:	8.9 (in.lb./rad.)
μ_{1v}	:	$.12129 \times 10^{2}$ (in./rad.)
K_{1f}	:	1615 (lb./in.)
K_{1v}	:	$-.10753$ (1/in.)
C_{Lf}	:	8.9 (lb.sec./in.)
C_{Lv}	:	$.15914 \times 10^{-2}$ (sec./in.)

The above relationships represent curve fits of experimental data, each tire parameter being measured as a function of V_o and N. The values of the constants in these relationships have been obtained from Collins and Black [11] and are listed in Table 2.

The Reference Case

To examine the effects on wheel shimmy of an out-of-true wheel and of normal load oscillations a "reference case" is first considered. For the reference case the wheel is true and the normal load is constant. The reference case provides a stability plot in the velocity-trail plane. The effects of the out of true wheel or the normal load oscillations on shimmy are determined by comparing the shimmy motions which result when these factors are included to the results for the reference case.

To obtain the stability plot for the reference case, the state equation of the system, Equation (21) is simplified by making the following choices of parameters:

(a) The wheel is perfect. (β, e_1, e_2, e_3 are zero)
(b) The road is flat. (δp is zero)

Using (a) and (b) above, the state equation reduces to three uncoupled sets of differential equations:

(1) A second order equation for the suspension deflection, η.
(2) An equation for wheel rotation, θ, which can be solved to yield

$$\theta = -\frac{V_o t}{R_e} \tag{23}$$

(3) A set of 4 first order differential equations which are linear in the state variables Δ, ψ_t, ψ, and $\dot{\psi}$.*

The set of equations in (3) may be written as

$$\frac{d\underset{\sim}{Y}}{dt} = [B]\underset{\sim}{Y} \tag{24}$$

where Y is a (4x1) state vector with components Δ, ψ_t, ψ, and $\dot{\psi}$ and [B] is the (4x4) matrix whose components B_{ij} are given by

$$B_{11} = 0$$
$$B_{12} = -V_o$$

* Several small linear terms were also neglected in Equation 21 in order to obtain Equation 24.

$$
\begin{aligned}
B_{13} &= -V_o\cos\nu \\
B_{14} &= -T\cos\nu \\
B_{21} &= (CK_1)/C_1 \\
B_{22} &= -(1+CC_L V_o)/C_1 \\
B_{23} &= -(CC_L V_o\cos\nu - C_2\sin\nu)/C_1 \\
B_{24} &= -(CC_L T\cos\nu)/C_1 \\
B_{31} &= 0 \\
B_{32} &= 0 \\
B_{33} &= 0 \\
B_{34} &= 1 \\
B_{41} &= (N_o\sin\nu + K_1 T\cos\nu)/I_\psi \\
B_{42} &= (\mu_1\cos\nu - V_o C_L T\cos\nu)/I_\psi \\
B_{43} &= (N_o\sin\nu\cos\nu T - V_o C_L\cos^2\nu)/I_\psi \\
B_{44} &= -(C_D + C_L T^2\cos^2\nu)/I_\psi
\end{aligned}
$$

The quantity T in the above relationships is the system trail given by

$$T = \frac{1}{\cos\nu}\left[(R_o - \frac{N_o}{K_T})\sin\nu - d\right] \tag{25}$$

The quantity N_o is a given constant normal load.

The trail is an important physical parameter in that it greatly influences the shimmy motions of the system. The trail is shown in Fig. 8 as the horizontal distance between P_1 and P_2, where P_1 is the point of intersection of the fork rotation axis and the ground and P_2 is the point on the ground directly beneath the axle, A (P_2 would be the tire contact point if the fork were pointing straight ahead with no lateral tire deflection).

The stability plot for the reference case is obtained from the eigenvalues of matrix [B] in Equation (24). The eigenvalues of B consist, at each point in the V_o-T plane, of two which are purely real and two which form a complex conjugate pair. The two real eigenvalues are negative at all points in the plane. Consequently, the shimmy oscillations are determined by the complex conjugate pair. The shimmy frequency, ω_s, is given by the magnitude of the imaginary parts and the exponential growth or decay rate of the shimmy oscillation, E_r, is given by the value of the real part. The shimmy motion is stable if E_r is negative, and unstable if E_r is positive. Both E_r and ω_s depend on V_o and T. In addition, ω_s increases monotonically as either V_o or T increase.

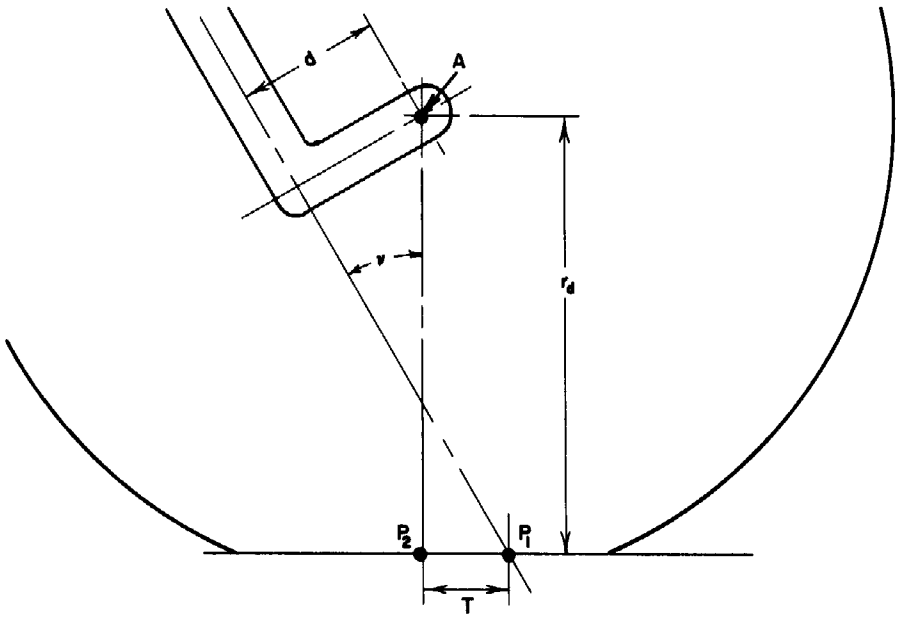

Fig. 8. Trail

Figure 9 shows a plot of the shimmy stability of the system as a function of V_o and T. For this plot the constants of Tables 1 and 2 were used, along with a normal load of 3100 lbs. This plot of shimmy stability will be used as the reference for comparison with other results.

The Effect of an Out-of-True Wheel on Wheel Shimmy

An out-of-true wheel ($\beta \neq 0$, see Fig. 3) causes an oscillatory lateral force to be applied by the road to the tire. This force arises due to the periodic lateral motion of the tire and due to the periodic change in the camber angle, γ. The oscillation occurs at the frequency of wheel rotation, ω_c. As a result a steady state shimmy is produced. The equation which describes this steady state shimmy is Equation (24) as modified by the addition of a forcing term. (The steady state shimmy exists if the homogeneous Equation 24 is stable.)

The magnitude of the steady state shimmy depends, for a given normal load, on V_o, T, and β. Fig. 10 shows the steady state shimmy magnitude $|\psi_{ss}|$, normalized with respect to β, as a function of V_o for three trails. These results were obtained by computer solution of Equation 21.

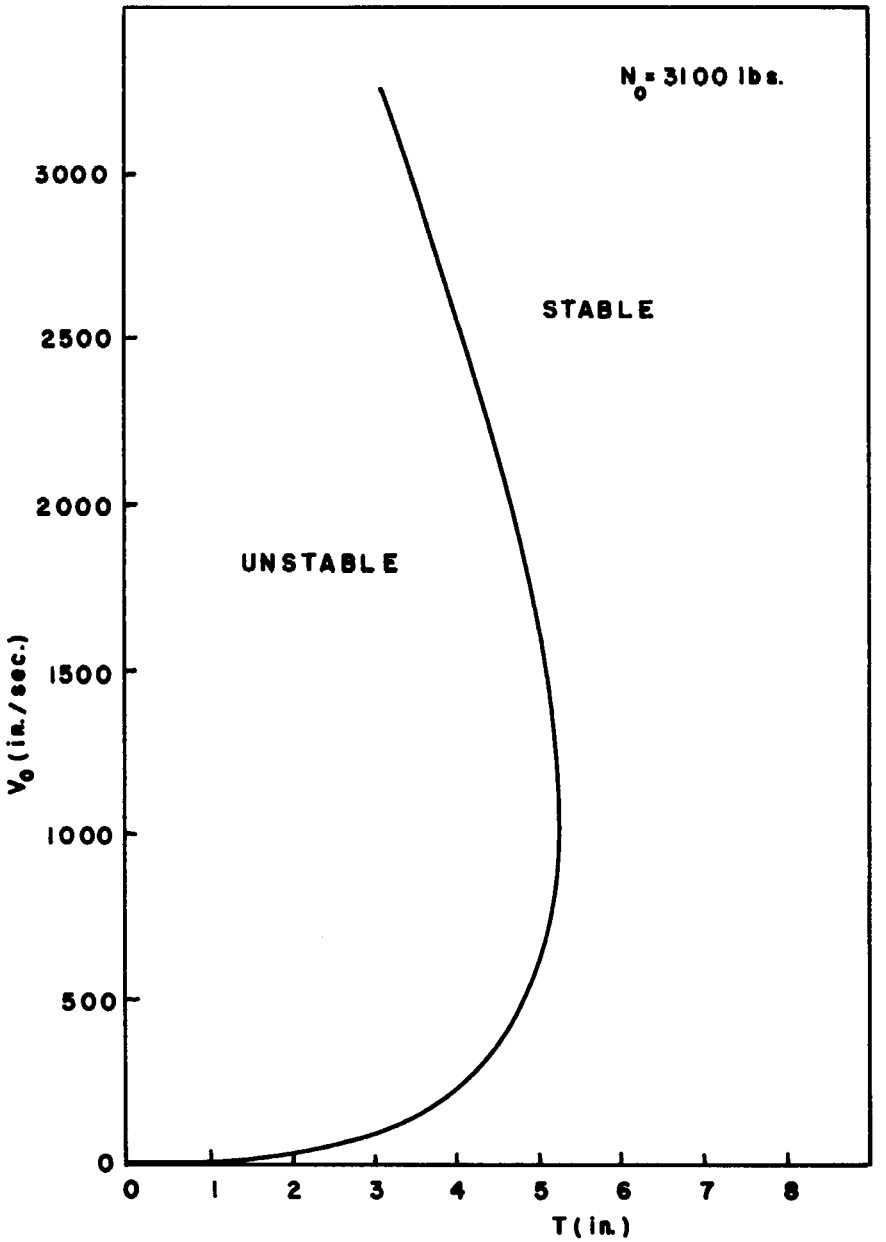

Fig. 9. Stability Diagram, Reference Case

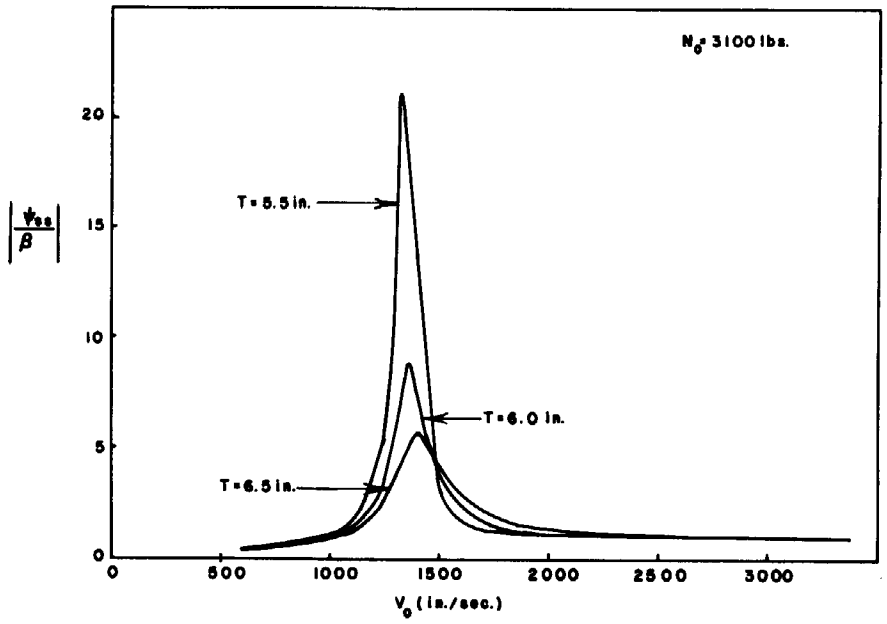

Fig. 10. Steady State Shimmy Magnitude

Fig. 10 shows that, for a given trail, the shimmy amplitude peaks at a certain velocity. The height of this peak depends on the trail (the height decreases as the trail increases). The peak occurs because a resonance condition exists. This resonance condition is produced when the frequency, ω_c, of the forcing function and the frequency, ω_s, of the free shimmy oscillation are approximately equal.

The velocity at which the resonance condition occurs can be determined approximately* by equating ω_c to ω_s. The rotation rate of the wheel ω_c is equal to that for the reference case and is given by

$$\omega_c = \frac{V_o}{R_e} \tag{26}$$

The shimmy frequency ω_s is obtained, as for the reference case, from the eigenvalues of [B] and is (for given N_o) a function of V_o and T; i.e., $\omega_s = \omega_s(V_o, T)$. For a given trail the velocity at which resonance will occur is obtained, approximately, by setting

$$\frac{V_o}{R_e} = \omega_s(V_o, T) \tag{27}$$

* The peak will not occur at exactly the velocity for which $\omega_c = \omega_s$ because of damping in the system.

Equation 27 provides a functional relationship between V_o and T; that is, a curve in the V_o, T plane near which resonance occurs. Fig. 11 shows this "resonance curve." Examination of both Figs. 10 and 11 shows that the resonance peaks do occur at points (V_o, T) which are close to the resonance line.

The Effect of Normal Load Oscillations on Wheel Shimmy

If the wheel is unbalanced (e_1 or $e_2 \neq 0$), if the tire is out of round ($e_3 \neq 0$) or if the road is rough ($\delta p \neq 0$), the normal load on the tire, N, is no longer constant but instead oscillates about some nominal value. For each of the above cases the normal load is obtained by solving the differential equation for suspension deflection. The total normal load is the sum of the normal loads for the three cases and is given by

$$N(t) = N_T(t) + N_o + N_1(t) + N_2(t) + N_3(t) \tag{28}$$

where $N_T(t)$ is the transient normal load, and where $N_1(t)$, $N_2(t)$, and $N_3(t)$ are the oscillatory normal loads caused by the unbalanced wheel, the out-of-round tire, and the rough road, respectively. Expressions for the above quantities are

$$N_T(t) = K_T \cos\nu e^{-\rho\omega_n t}[d_1\cos(\omega_d t) + d_2\sin(\omega_d t)]$$

$$N_o = K_s K_T [R_o - h - d\sin\nu + L_f\cos\nu]/[K_s + \cos^2\nu K_T] \tag{29}$$

$$N_1(t) = \frac{m_w\omega_c^2\sqrt{e_1^2 + e_2^2}}{\sqrt{d_3^2 + d_4^2}}\cos(-\omega_c t - \Phi_1)$$

$$N_2(t) = K_T e_3\left[1 - \left(\frac{K_T\cos^2\nu d_3}{\sqrt{d_3^2+d_4^2}}\right)^2 + \left(\frac{K_T\cos^2\nu d_4}{\sqrt{d_3^2+d_4^2}}\right)^2\right]^{1/2}\cos(-\omega_c t - \Phi_2)$$

$$N_3(t) = K_T\delta_p\left[1 - \left(\frac{K_T\cos^2\nu d_5}{\sqrt{d_5^2+d_6^2}}\right)^2 + \left(\frac{K_T\cos^2\nu d_6}{\sqrt{d_5^2+d_6^2}}\right)^2\right]^{1/2}\cos(\omega_r t - \Phi_3)$$

where d_1 and d_2 are constants determined by initial conditions on the suspension deflection and where ω_r, d_3, d_4, d_5, and d_6 are given by

$$\omega_r = \frac{2\pi V_o}{\lambda}$$

$$d_3 = K_s + \cos^2\nu K_T - (m_f + m_w)\omega_c^2$$

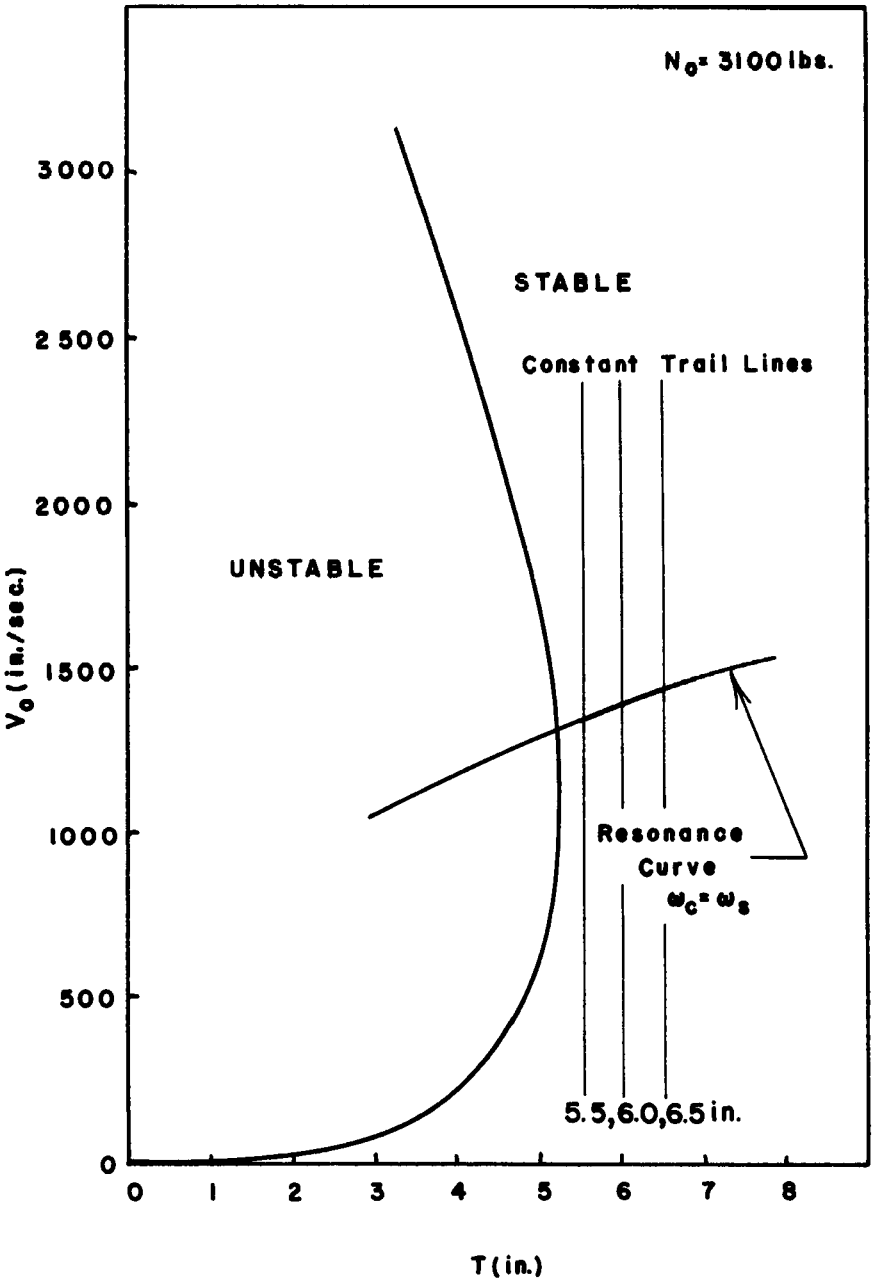

Fig. 11. Resonance Curve $\omega_c = \omega_s$

$$d_4 = C_s\omega_c$$

$$d_5 = K_s + \cos^2\nu K_T - (M_f + m_w)\,\omega_r^2$$

$$d_6 = C_s\omega_r$$

Quantities Φ_1, Φ_2, and Φ_3 are phase angles.

Under steady operating conditions, the normal load N(t) consists of N_o, $N_1(t)$, $N_2(t)$, and $N_3(t)$. An expression for N(t) having the form

$$N(t) = N_o + \delta_N \cos(\omega t - \Phi) \tag{30}$$

can be used to represent the combination of N_o with $N_1(t)$, $N_2(t)$, or $N_3(t)$. In this expression, δ_N is the magnitude of the normal load oscillation, ω and Φ its frequency and phase. For each case, δ_N and ω may be obtained from Equation 29.

Shimmy oscillations for any of the three cases are governed by Equation 24 in which N_o is replaced by N(t) from Equation 28. Equation 24 then contains periodic coefficients. The growth-decay behavior of the shimmy oscillations (and thus the stability of the system) can be investigated by the use of Floquet theory [17]. From the application of the theory to Equation 24*, the four exponential growth-decay rates are

$$E_i = \frac{\ell n|\xi_i|}{P} \qquad i = 1, 2, 3, 4 \tag{31}$$

In Equation 31, ξ_i, i = 1, 2, 3, 4 are the four eigenvalues of [W(P)]. Matrix [W(P)] is the fundamental solution matrix** of Equation 24 (evaluated at t = P, where P is the period of the elements of [B]). The growth-decay behavior of the solutions to Equation 24 is dominated by the algebraically largest of the rates given by Equation 31. If this rate, $E_{max.}$, is negative, then the system is stable. If this rate is positive, the system is unstable.

In addition to Floquet theory, computer simulation*** can be used to determine the growth-decay behavior of the shimmy oscillations. Both Floquet theory and simulation were used to obtain the results which follow. Simulation was employed primarily to check the Floquet theory results.

---

* See [15].

** The fundamental solution matrix of Equation 24 is the matrix whose columns are solution vectors of (24) and which is equal to the identity matrix when t = 0.

*** Simulation can be more accurate than Floquet theory because simulation does not require making the approximations used obtain Equation 24.

Since for any of the three cases the normal load is described by Equation 30, it is sufficient to consider the effect on shimmy stability of an arbitrary normal load oscillation; i.e., δ_N and ω are considered arbitrary parameters. Figure 12 shows three curves of E_{max} vs. (ω/ω_s) for δ_N constant. Each curve corresponds to a point in the V_o-T plane. The graphs indicate that the stability of the system is affected by the normal load oscillation only when

$$(\frac{\omega}{\omega_s}) \approx 2$$

Thus, whenever the frequency of the normal load oscillation is close to twice the natural shimmy frequency, the stability of the system is decreased.

Figure 13 shows curves of E_{max} vs. (δ_N/N_o) for $(\omega/\omega_s) = 2$. The three curves given correspond to those points in the V_o-T plane used for Figure 12. These curves show that an increase in the magnitude of the normal load oscillation yields a decrease in the stability of the shimmy.

To determine the cause of the decrease in stability it is necessary to examine how the normal load enters into the problem. The normal load enters into the equation which describes wheel shimmy (Equation 24) in two ways: directly as a term in matrix [B] and indirectly due to the variation of tire constants with normal load (see Equations 22). When the normal load oscillates, both of these effects

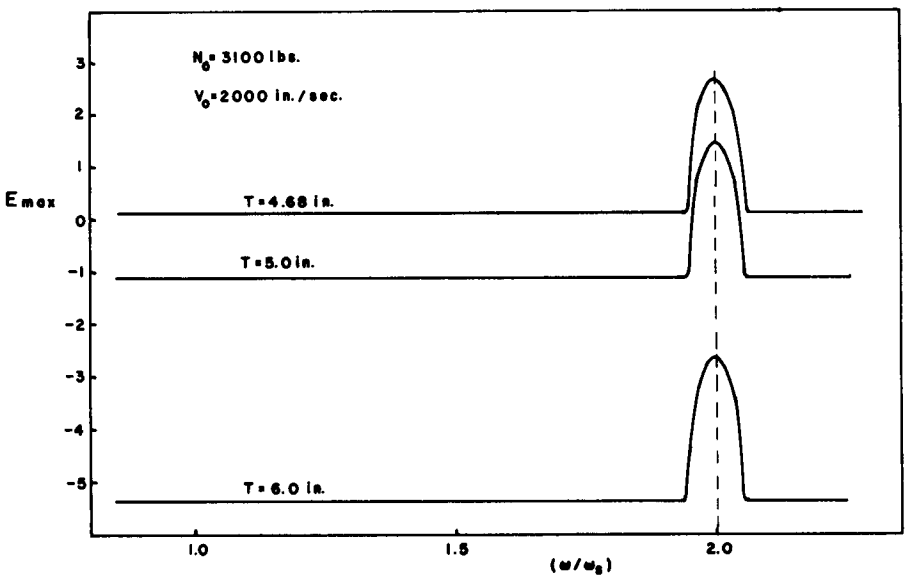

Fig. 12. Effect of Normal Load Oscillation Frequency on Stability

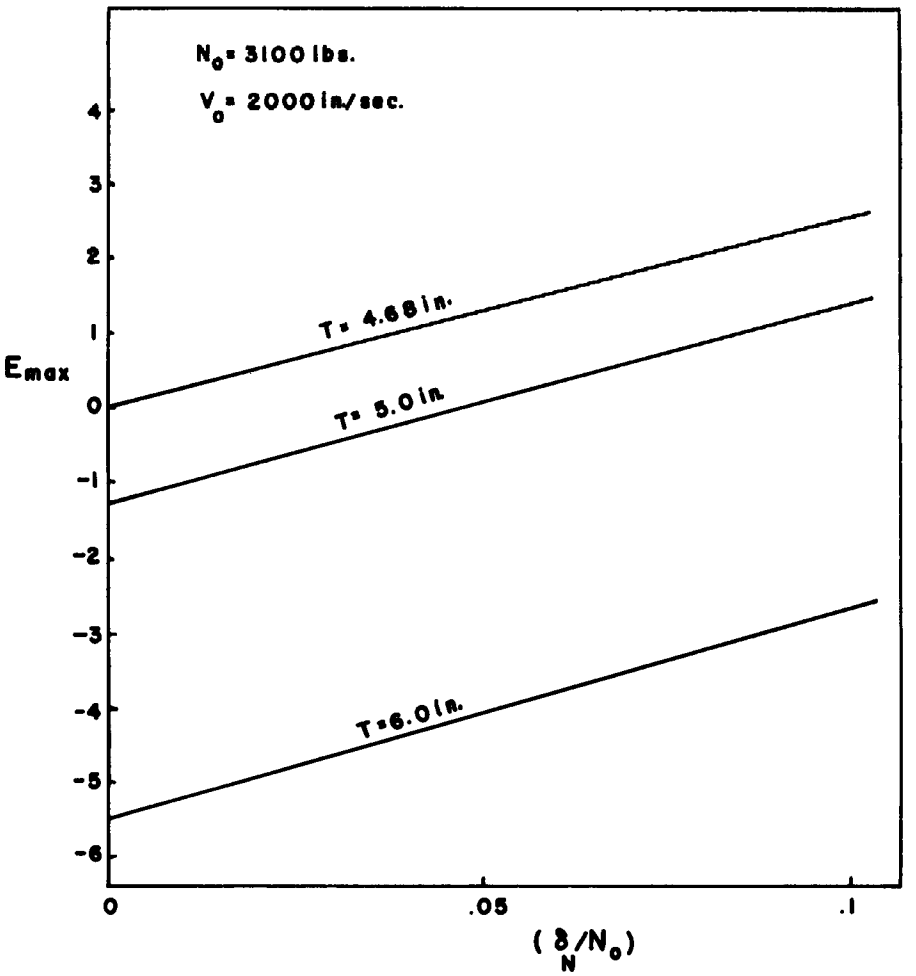

Fig. 13. Effect of Normal Load Oscillation Magnitude on Stability

contribute to the loss of stability shown in Figures 12 and 13. To separate the two effects, the values given for the tire parameters in Table 2 were modified. Seven cases were considered:

A. Tire constants same as in Table 2.

B. Tire constants independent of normal load.

$$(K_{1v} = C_{Lv} = \mu_{1v} = C_{1v} = C_{1vv} = C_v = C_{2v} = 0)$$

C. Only C varies with normal load.

$$(K_{1v} = C_{Lv} = \mu_{1v} = C_{1v} = C_{1vv} = C_{2v} = 0)$$

D. Only C_l varies with normal load.

$$(K_{lv} = C_{Lv} = \mu_{lv} = C_v = C_{2v} = 0)$$

E. Only μ_l varies with normal load.

$$(K_{lv} = C_{Lv} = C_{lv} = C_{lvv} = C_v = C_{2v} = 0)$$

F. Only C_L varies with normal load.

$$(K_{lv} = \mu_{lv} = C_{lv} = C_{lvv} = C_v = C_{2v} = 0)$$

G. Only K_l varies with normal load.

$$(C_{Lv} = \mu_{lv} = C_{lv} = C_{lvv} = C_v = C_{2v} = 0)$$

The system stability associated with each of the seven cases above was studied by plotting for constant δ_N/N_0, $E_{max.}$ vs. ω at one point in the V_0-T plane. These plots are shown in Fig. 14. The results indicate that the effect on stability of the normal load variation alone, without the variation of the tire parameter values, is very small but does decrease the stability somewhat. Thus, the major reason for the decrease in stability is the variation of the tire parameter values with normal load. In particular, the variation of the cornering stiffness of the tire with normal load has the greatest effect on stability for the system considered.

As an example of this loss of stability, the case of a statically unbalanced wheel was considered. A stability diagram (obtained with Floquet theory) for the system

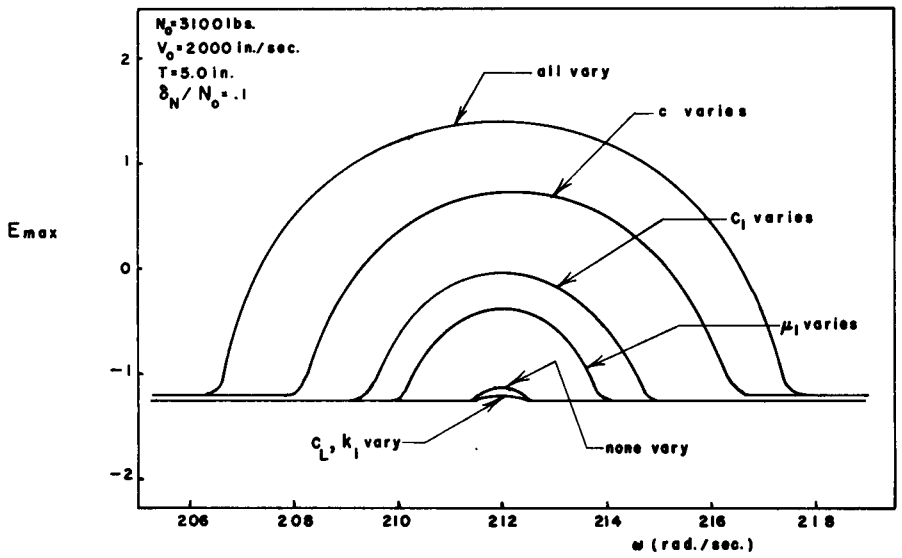

Fig. 14. Effect of Tire Constant Assumptions on Stability

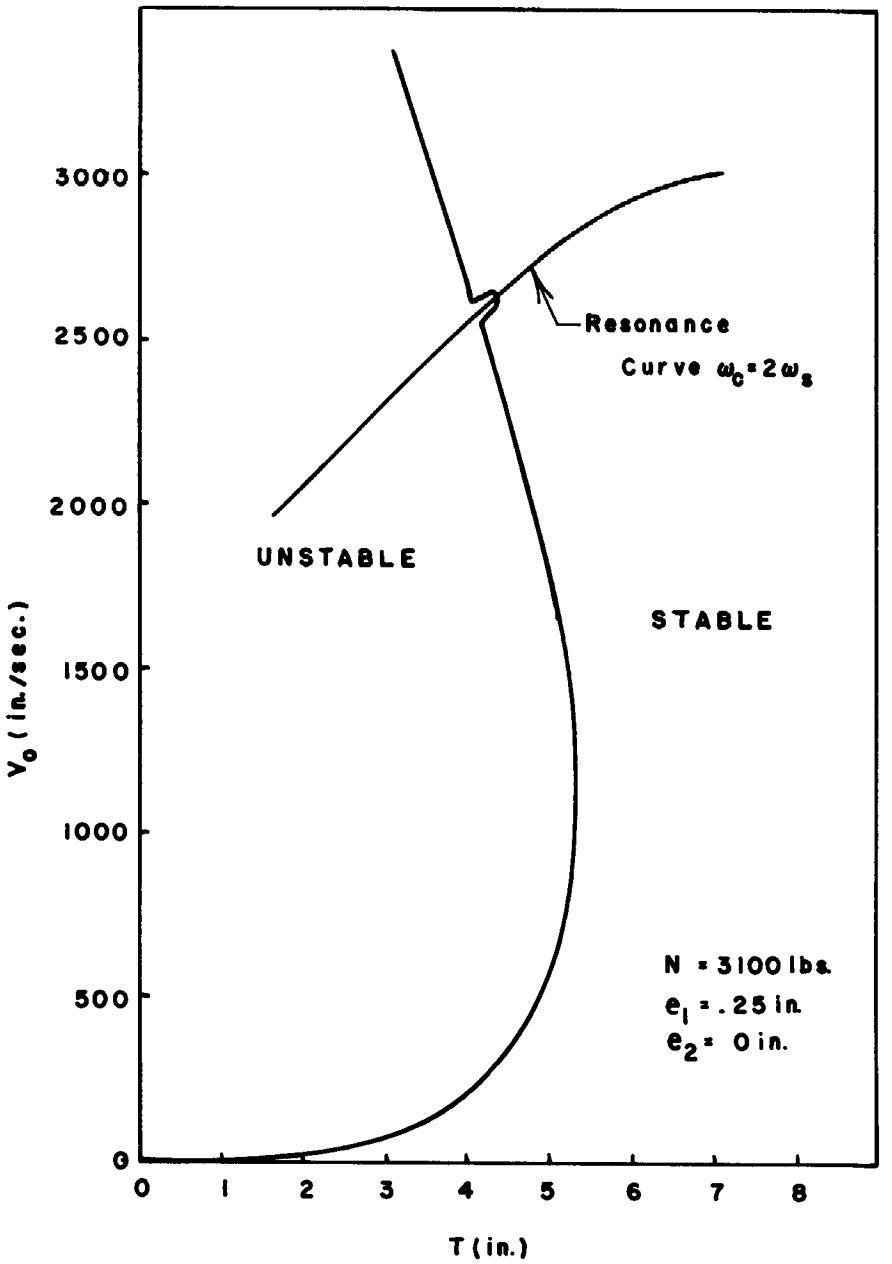

Fig. 15. Stability Diagram, Unbalanced Wheel

with $e_1 = .25"$, $e_2 = 0"$ is shown in Fig. 15. This diagram is identical to the one for the reference case except for the small additional region of instability in the upper portion of the diagram. This new region of instability is centered on a (parametric) resonance curve for which ω_c* is equal to $2\omega_s$. The resonance curve is defined in the V_o, T plane by

$$\frac{V_o}{R_e} = 2\omega_s(V_o, T)$$

A loss of system stability occurs all along the resonance curve. If the inherent stability (that associated with the reference case) is small, then a static imbalance causes the system to be unstable. However, if the inherent stability is high the system does not go unstable due to the static imbalance, but the degree of stability (as indicated by the exponential decay rate) decreases. Figure 16 shows a graph, obtained by use of Floquet theory with Equation 24, of $E_{max.}$ as a function of position along the resonance curve $\omega_c = 2\omega_s$. The figure also gives the results for the reference case. Superimposed on this graph are the growth-decay rates obtained by simulation. The Figure shows the decrease in stability caused by the static imbalance. Good agreement between the Floquet theory and simulation results is also shown.

A graph of $E_{max.}$ as a function of V_o for constant T is shown in Fig. 17. The expected decrease in stability (increase in $E_{max.}$) when V_o is close to the resonance curve is clearly indicated in the Figure.

In addition to the effects described above, a loss of stability in the region of the V_o-T plane centered on the (parametric resonance curve $\omega_c = 2\omega_s$ would be produced by an out of round tire. A road whose profile varies with wave length λ also produces a loss of stability centered on a (parametric) resonance curve. For this case, the equation for the resonance curve is

$$\omega_r = \frac{2\pi V_o}{\lambda} = 2\omega_s(V_o, T)$$

The Effect of Accelerations and Braking-Traction Forces on Wheel Shimmy

The cases of constant system acceleration and of constant braking-traction forces are discussed in [15]. The effect of acceleration on shimmy motion was found to be negligible. The shimmy motion decayed whenever the point defined by the instantaneous velocity and the trail was in a stable region of Figure 9, and increased

* The normal load oscillation frequency for this case is the rotation rate of the wheel, ω_c.

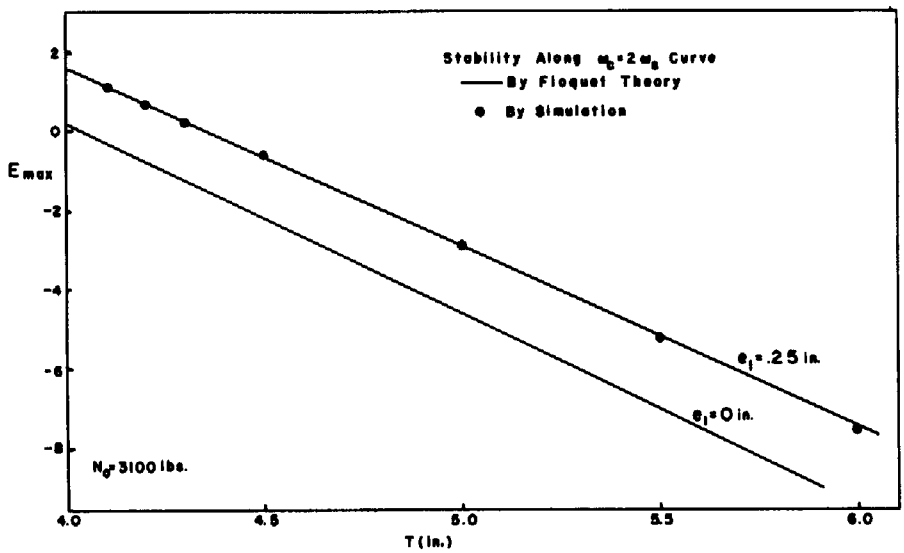

Fig. 16. Stability on $\omega_c = 2\omega_s$

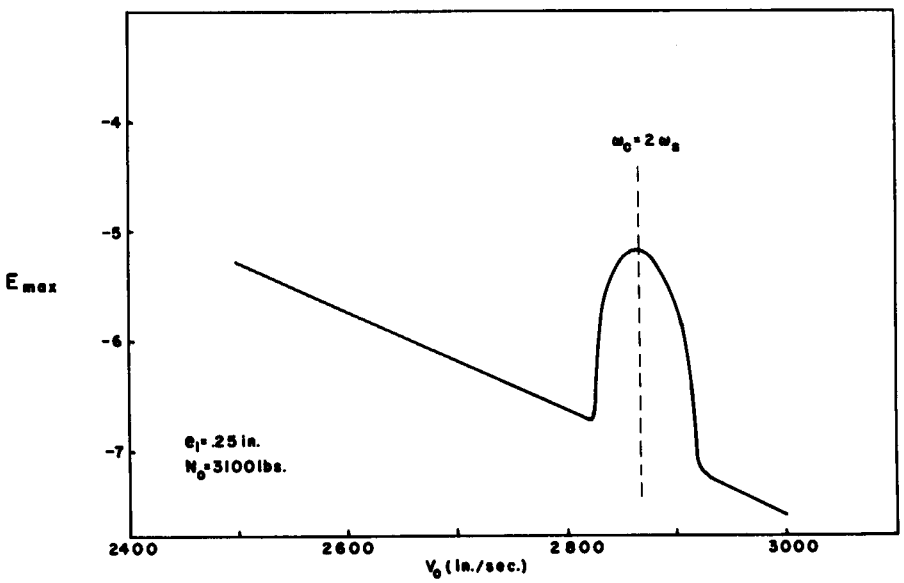

Fig. 17. Stability at Constant Trail

whenever the point was in an unstable region. The effect of braking-traction forces that was considered was the torque exerted by these forces whenever the tire is deflected sideways. They were found to alter the system's stability slightly. Braking forces stabilized the system, traction forces destabilized it. These changes, however, were so small (for the cases examined) as to be negligible when compared to the shimmy behavior associated with the reference case.

4. SUMMARY AND CONCLUSIONS

This paper has examined the effects of several system factors on wheel shimmy. The results obtained are as follows. An out-of-true wheel causes a steady-state shimmy at the frequency of wheel rotation. When this frequency is close to the shimmy frequency, resonance occurs and a large steady-state shimmy amplitude can result. This resonance occurs at a forward velocity equal to a "resonance velocity" which is a function of trail for a given system.

A normal load oscillation whose frequency is close to twice the shimmy frequency decreases the stability of the system. This loss of stability is due primarily to the variation of tire parameters with normal load. Tire-wheel irregularities such as imbalance and out of roundness cause normal load oscillations whose frequency is the frequency of wheel rotation. Thus, when the frequency of wheel rotation is close to twice the shimmy frequency a loss of stability results. The velocity at which this loss of stability occurs is a function of the trail for the given system.

Road surface roughness also causes normal load oscillations whose frequencies depend on the system speed and on the wavelength of the road profile. A loss of stability results when one of these frequencies is close to twice the shimmy frequency.

Braking-traction forces have a small effect on system stability. A braking force increases the stability and a traction force decreases it. A constant system acceleration has a negligible effect on shimmy stability.

The results of this paper indicate the existence of factors whose presence may degrade the performance of an otherwise satisfactory steerable pneumatic tire system. The designer of such a system should be aware of these factors and of their effects on wheel shimmy. The designer can avoid these effects by designing the system such that the various resonance occur at speeds which are out of the operating range. Alternatively he can compensate for the effects by increasing the inherent system stability.

REFERENCES

1. von Schlippe, B. and R. Dietrich. "Das Flattern eines bepneuten Rades," (Shimmying of a Pneumatic Wheel) Bericht 140, L.G.L., 1941, pp. 35-45, 63-66. (Available in English translation in NACA TM 1365, 1954, pp. 125-160, 217-228.)
2. Smiley, R. F. "Correlation, Evaluation, and Extension of Linearized Theories for Tire Motion and Wheel Shimmy," NACA Report 1299, 1957.
3. Segel, L. "Force and Moment Response of Pneumatic Tires to Lateral Motion Inputs," Transactions ASME, *Journal of Engineering For Industry*, 88 B, 1966, p.8
4. Pacejka, H. B. "Approximate Dynamic Shimmy Response of Pneumatic Tires," *Vehicle System Dynamics*, 2, 1973, pp. 49-60.
5. Pacejka, H. B. "Analysis of the Shimmy Phenomenon," *Proceedings of the Institute for Mechanical Engineers*, Vol. 180, Pt. 2A, No. 10, pp. 251-268.
6. Pacejka, H. B. "The Wheel Shimmy Phenomenon," Ph.D. Thesis, Delft University of Technology, 1966.
7. Fromm, H.: Kurzer Bericht über die Geschichte der Theorie des Radflatterns," (Brief Report on the History of the Theory of Wheel Shimmy) Bericht 140, L.G.L., 1941, pp. 53-56. (Available in English translation in NACA TM 1365, pp. 181-190.)
8. Bourcier de Carbon, Christian. "Etude Théorique du Shimmy des Roues d'Avion," (Analytical Study of Shimmy of Airplane Wheels) Office National d'Etudes et de Recherches Aéronautiques, Publication No. 7, 1948. (Available in English translation in NACA TM 1337, 1952.)
9. Moreland, W. J. "Landing Gear Vibration," Air Force Technical Report No. 6590, Wright Air Development Center, U.S. Air Force, October, 1951.
10. Moreland, W. J. "The Story of Shimmy," *Journal of the Aeronautical Sciences*, Vol. 21, No. 12 (December 1954) pp. 793-808.
11. Collins, R. L. and R. J. Black. "Tire Parameters for Landing Gear Shimmy Studies," *Journal of Aircraft*, Vol. 6, No. 3, May-June 1969, pp. 252-258.
12. Collins, R. L., "Theories on the Mechanics of Tires and Their Applications to Shimmy Analysis," *Journal of Aircraft*, Vol. 8, No. 4, April 1971, pp. 271-277.
13. Schrode, H. "Verminderung der Flatterneigung von Sporn-und Bugwerken durch Einbau besonders ger formter Reifen," (Reduction of the Shimmy Tendency of Tail and Nose-Wheel Landing Gears by Installation of Specially Designed Tires) Tech. Berichte, Bd. 10, Heft 4, ZWB, April 15, 1943, pp. 113-116. (Available in English translation as NACA TM 1391, 1955).
14. Ho, F. H. and J. L. Lai. "Parametric Shimmy of a Nosegear," *Journal of Aircraft*, Vol. 7, No. 4, pp. 373-375.
15. Podgorski, W. A. "The Wheel Shimmy Problem: Its Relationship to Longitudinal Tire Forces, Vehicle Motions, and Normal Load Oscillations", Ph.D. Thesis, Cornell University, 1974.
16. Smiley, R. F. and W. B. Horne. "Mechanical Properties of Pneumatic Tires with Special Reference to Modern Aircraft Tires," NASA Technical Report R-64, 1960.
17. Cesari, L. "Asymptotic Behavior and Stability Problems in Ordinary Differential Equations," Springer-Verlag: New York, 1971, pp. 55-79.